Analysis of the meson-meson data in the framework of the dispersion *D*-matrix method

A. V. Anisovich, V. A. Nikonov, and A. V. Sarantsev
Petersburg Nuclear Physics Institute, Gatchina, Russia and Helmholtz-Institut für Strahlen-und Kernphysik, Universität Bonn, Germany

V. V. Anisovich, M. A. Matveev, and T. O. Vulfs
Petersburg Nuclear Physics Institute, Gatchina, Russia

K. V. Nikonov
Petersburg State University, Department of Physics, St. Petersburg, Russia

J. Nyiri
Research Institute for Particle and Nuclear Physics, Budapest, Hungary
(Received 21 June 2011; revised manuscript received 10 August 2011; published 5 October 2011)

We describe the meson-meson data for the ($IJ^{PC} = 00^{++}$) wave at $280 \leq \sqrt{s} \leq 1900$ MeV in two approaches: (i) the K-matrix approach and (ii) the dispersion relation D-matrix method. With a good description of low-energy data (at $280 \leq \sqrt{s} \leq 900$ MeV) as well as the data of two-meson transition amplitudes and antiproton-proton annihilation into three pseudoscalar meson states (at $450 \leq \sqrt{s} \leq 1950$ MeV) we have found the positions of the resonance poles: (i) for the σ meson pole: $M_\sigma = (390 \pm 35) - i(235 \pm 50)$ MeV; (ii) two poles for the $f_0(980)$, on the second sheet (under the $\pi\pi$ cut): $M_I = (1011 \pm 5) - i(35 \pm 5)$ MeV, and on the third sheet (under the $\pi\pi$ and $K\bar{K}$ cuts), $M_{II} = (1035 \pm 50) - i(460 \pm 50)$ MeV; for the $f_0(1370)$ meson, $M = (1285 \pm 30) - i(160 \pm 20)$ MeV; for the $f_0(1500)$ meson, $M = (1488 \pm 4) - i(53 \pm 5)$ MeV; for the $f_0(1790)$ meson, $M = (1775 \pm 25) - i(140 \pm 15)$ MeV; and for the broad state $f_0(1200\text{–}1600)$ $M = (1540 \pm 120) - i(550 \pm 70)$ MeV. Our estimation of the scalar-isoscalar scattering length obtained under different parameterizations and assumptions about the quality of low-energy $\pi\pi$ scattering data is $a_0^0 = (0.215 \pm 0.040) m_\pi^{-1}$. We also discuss the idea according to which the σ meson could be a remnant of the confinement singularity, $1/s^2$, in a white channel.

DOI: 10.1103/PhysRevD.84.076001 PACS numbers: 11.55.Fv, 11.80.Et, 13.75.Lb, 14.40.Rt

I. INTRODUCTION

In spite of lengthy and persistent investigations, at present we have no firm determination for the mass of the σ meson—the resonance in the 280–900 MeV region. This resonance reveals itself in the $\pi\pi$ channel as a pole in the complex-M plane, in the ($IJ^{PC} = 00^{++}$) partial wave. Numerous calculations produced mass values distributed over all the low-energy interval $\sqrt{s} \equiv M \lesssim 900$ MeV, with various widths from 200 MeV up to 1000 MeV. Such a situation emerged in the nineties [1]. The results of the latest analyses are clustered in a smaller mass region 400–600 MeV: see, for example, [2] $(552^{+84}_{-106}) - i(232^{+81}_{-72})$ MeV and [3] $(484 \pm 17) - i(255 \pm 10)$ MeV and the review of Bugg [4] $(472 \pm 30) - i(271 \pm 30)$ MeV. The solution of the Roy equation at low energies produced a smaller mass (441^{+16}_{-8}) MeV $- i(272^{+9}_{-13})$ MeV [5]. A detailed investigation of theoretical uncertainties in the parametrization of the low-energy data is given in [6].

We see three sources for emerging uncertainties in the analyses of the $\pi\pi$ amplitude near the threshold:

(i) a not sufficiently good determination of the 00^{++} amplitude above $M = 900$ MeV
(ii) uncertainties in the definition of the left-hand cut in the $\pi\pi$ amplitude and
(iii) uncertainties in low-energy $\pi\pi \to \pi\pi$ data.

In the present paper we analyzed in detail all these sources of uncertainties. The examples considered in the paper demonstrate that the results obtained for the low-energy amplitude depend strongly on the assumptions made in the analysis.

A very important source of the information about the isoscalar-scalar partial wave is the proton-antiproton annihilation at rest into three pseudoscalar mesons. In the $\bar{p}p \to 3\pi^0$ reaction on the liquid hydrogen the S-wave annihilation contributes about 94% to the decay rate and the scalar-isoscalar partial wave about 75%. The analysis of the Dalitz plot provides a possibility to study interferences of the high-mass contributions with low-mass contributions produced in different kinematic channels. The first analyses of the Crystal Barrel data for this reaction was reported in [7]. A good compatibility of the obtained solution with the elastic data extracted by the CERN-Munich group [8] was demonstrated in [9]. The analysis of the proton-antiproton data allows us to extract the states with a small inelasticity which can escape an identification

from the analysis of the elastic channel alone (see for example [10]). In the paper [11] the elastic data were analyzed together with central production data. However, the analysis of such data is a rather complicated task and this is probably the reason why the obtained spectrum is not fully compatible with that observed in the analysis of the proton-antiproton annihilation data.

The meson spectra in the 00^{++} wave were fitted by our group using the K-matrix technique in [12–14]. This technique provides us with an opportunity to fit simultaneously several reactions (such as $\pi\pi$, $K\bar{K}$, $\eta\eta$, etc.), taking into account correctly analytical properties and unitarity in all investigated amplitudes. This way we have determined the resonance structure of the scalar-isoscalar wave at $500 \leq \sqrt{s} \leq 1950$ MeV; our results were summarized in [15].

However, in the K-matrix amplitude the left-hand cut owing to crossing channels is determined ambiguously (note that t and u channel meson exchanges depend on couplings and form factors, which are not well known). The impossibility to write down precisely the contributions of left-hand cuts leads to a freedom in the interpretation of the $\pi\pi \to \pi\pi$ amplitude in the $\sqrt{s} < 500$ MeV region. In our K-matrix analyses [12–14] of the isoscalar-scalar wave we modeled the contribution from the left-hand cut at $s < 0$ by introducing several poles in this region with fitted parameters. Describing this partial amplitude in the region $280 \leq \sqrt{s} \leq 1900$ MeV, we usually did not observe a pole which could be interpreted as the σ meson. However, in some solutions (not the best ones) such a pole appeared.

Having this background, we fitted in [16] the amplitude 00^{++} in the region $280 \leq \sqrt{s} \leq 900$ MeV separately in the framework of the dispersion relation approach sewing the N/D solution with the K-matrix one at $450 \leq \sqrt{s} \leq 900$ MeV. As a result, the best fit, accounting for the left-hand cut contribution (it was a fitting function), contained the σ-meson pole at $M_\sigma = (430 \pm 150) - i(320 \pm 130)$ MeV [16].

One can think that the ambiguity problem may be solved with the help of the investigation of the $\pi\pi$ scattering in all three (u, d, s) channels (see [5,17] and references therein). However, this procedure requires the analytical continuation of the pole terms into regions being rather far from the pole mass. This supposes the knowledge not only of both resonance form factors and the energy dependence of resonance widths. The high spin states lead to the divergence in crossing channels. It is only the summing over all sets of states that resolves these divergences resulting finally in the Regge behavior and therefore, requires model-dependent calculations.

The K-matrix analysis [12–14], being performed at a distance from the left-hand cut, gives masses and full widths of resonances (i.e. the position of poles) as well as the residues of the poles, namely, couplings of resonances to different channels. These couplings are factorized; this is a criterium for dealing just with a particle, though unstable. Besides, the coupling interrelations allow one to define the quark content of a particle, provided this is a $q\bar{q}$ state. This way the states found in the K-matrix analysis can be classified as $q\bar{q}$ nonets. The K-matrix analysis determines two nonets and one extra state in the 600–2000 MeV region. One of the possible classifications is given in [15]:

$$[f_0(980), f_0(1300)]_{n=1}, \qquad [f_0(1500), f_0(1750)]_{n=2};$$

where $n = 1, 2$ are the radial quantum numbers. Here the broad state $f_0(1200–1600)$ and the σ-meson are superfluous for the $q\bar{q}$ nonet classification. The position of resonances in the $IJ^{PC} = 00^{++}$ wave is shown in Fig. 1.

In this classification the broad state $f_0(1200–1600)$ is a glueball descendant [18,19]. Because of another classification the broad $f_0(1200–1600)$ state belongs to the first nonet and the extra state is $f_0(1300)$. Both these states are flavor blind and one of them is superfluous for the $q\bar{q}$ systematics. The $f_0(1200–1600)$ state acquired a large width because of the accumulation of widths of neighboring states: in nuclear physics such a phenomenon had been studied in [20–22], in meson physics in [23].

The paper is organized as follows. In Sec. II we provide formulae used in the K-matrix and D-matrix approaches. In Sec. III we discuss an idea of the confinement singularity $1/s^2$. Such a singularity in the t channel $(1/t^2)$ corresponds to the linear rising potential which describes meson spectra in $q\bar{q}$ [24], $b\bar{b}$ [25] and $c\bar{c}$ [26] channels and gives correct values for the partial widths of radiative and hadronic decays of confined $q\bar{q}$ states [27]. Although this singularity is expected to be in the color octet state, it can have also a color singlet component and appear in

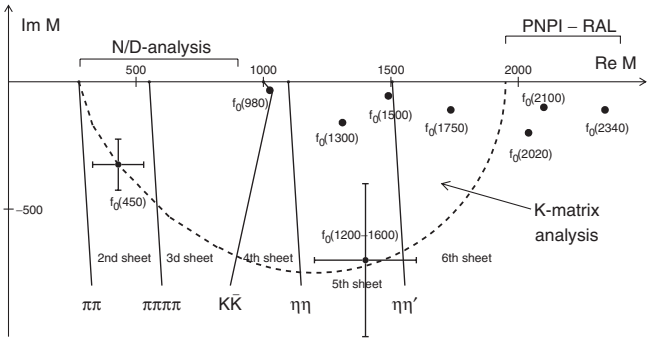

FIG. 1. Complex-M plane for the $(IJ^{PC} = 00^{++})$ mesons [15]. The dashed line encircles the part of the plane where the K-matrix analysis [13] reconstructs the analytical K-matrix amplitude: in this area the poles corresponding to resonances $f_0(980)$, $f_0(1300)$, $f_0(1500)$, $f_0(1750)$ and the broad state $f_0(1200–1600)$ are located. Beyond this area, in the low-mass region, the pole of the light σ meson is located (shown by the point the position of pole, $M = (430 - i320)$ MeV, corresponds to the result of N/D analysis; the crossed bars stand for σ-meson pole found in [16]. In the high-mass region one has resonances $f_0(2030)$, $f_0(2100)$, $f_0(2340)$, see [39]. Solid lines stand for the cuts related to the thresholds $\pi\pi$, $\pi\pi\pi\pi$, $K\bar{K}$, $\eta\eta$, $\eta\eta'$.

the s channel. The K-matrix and D-matrix analyses of the 00^{++} wave in the energy interval $280 \le \sqrt{s} \le 1900$ MeV are presented in Sec. IV. In the Conclusion we summarize the results concentrating on the low-energy region.

Some clarifying points are made in the Appendices. In Appendix A the dynamical mechanism of the singularity $1/s^2$ in the $q\bar{q} \to q\bar{q}$ amplitude is discussed. A simple description in terms of the dispersion relation approach which allows to incorporate easily the singularity $1/s^2$ into the analytic and unitary amplitudes is given in Appendix B. In Appendix C we present the unitary $\pi\pi$ scattering in the threshold regions taking into account the mass differences of the $\pi^+\pi^-$ and $\pi^0\pi^0$ systems which are essential for the extraction of a_0^0.

II. THE K-MATRIX AND D-MATRIX TECHNIQUES

Here we discuss the analytic properties of amplitudes restored in terms of the K-matrix and D-matrix techniques.

The comparison of results obtained by these two methods is one of the main subject of the present investigation. In the K-matrix approach the real part of loop diagrams is neglected, or, more precisely, is taken into account effectively as renormalization of resonance masses. In the D-vector approach, real parts of loop diagrams are calculated directly and amplitude does not have false kinematical singularities in the region of left-side singularities.

Although the D-matrix method is theoretically better founded, the majority of the partial wave analyses are performed in the framework of the K-matrix approach and a good understanding of stability and limitations of the obtained results is an important task.

A. The K-matrix approach

For the S-wave interaction in the isoscalar sector we use, as previously [13], the 5-channel K-matrix:

$$K_{ab}(s) = \left(\sum_\alpha \frac{g_a^{(\alpha)} g_b^{(\alpha)}}{M_\alpha^2 - s} + f_{ab}\frac{1\ \mathrm{GeV}^2 + s_0}{s + s_0}\right)\frac{s - s_A}{s + s_{A0}}, \quad (1)$$

where K_{ab} is a 5×5 matrix ($a, b = 1, 2, 3, 4, 5$), with the following notations for meson states: $1 = \pi\pi$, $2 = K\bar{K}$, $3 = \eta\eta$, $4 = \eta\eta'$ and $5 =$ multimeson states (four-pion state mainly at $\sqrt{s} < 1.6$ GeV). The $g_a^{(\alpha)}$ are coupling constants of the bare state α to meson channels; the parameters f_{ab} and s_0 describe the smooth part of the K-matrix elements ($s_0 > 1.5$ GeV^2). The factor $(s - s_A)/(s + s_{A0})$, where $s_A \sim (0.1\text{–}0.5)m_\pi^2$, describes Adler's zero in the two-pion channel. However, in the K-matrix analysis we introduced this factor also in other channels to suppress the effect of the left-hand side false kinematic singularities in the K-matrix amplitude.

Spectral integral equation for the K-matrix amplitude

Discussing meson-meson scattering and production amplitudes, we use the dispersion relation (or spectral integral) technique. In terms of this technique we write for the K-matrix amplitude a spectral integral equation which is an analog of the Bethe-Salpeter equation [28] for the Feynman technique. The spectral integral equation for the transition amplitude from the channel a to channel b is presented graphically in Fig. 2 and reads:

$$A_{ab}(s) = \int \frac{ds'}{\pi}\frac{A_{aj}(s, s')}{s' - s - i0}\rho_j(s')K_{jb}(s', s) + K_{ab}(s). \quad (2)$$

Here $\rho_j(s')$ is the diagonal matrix of the phase volumes, $A_{aj}(s, s')$ is the off-shell amplitude and $K_{jb}(s, s')$ is the off-shell elementary interaction. Let us remind that in the dispersion relation technique, just as in quantum mechanics, there is no energy conservation for the intermediate states.

The standard way of the transformation of Eq. (2) into the K-matrix form is the extraction of the imaginary and principal parts of the integral. The principal part has no singularities in the physical region and can be omitted (or taken into account by a renormalization of the K-matrix parameters):

$$\begin{aligned}&\int \frac{ds'}{\pi}\frac{A_{aj}(s, s')}{s' - s - i0}\rho_j(s')K_{jb}(s', s)\\ &= P\int \frac{ds'}{\pi}\frac{A_{aj}(s, s')}{s' - s}\rho_j(s')K_{jb}(s', s) + iA_{aj}(s, s)\rho_j(s)K_{jb}(s)\\ &\quad \to iA_{aj}(s, s)\rho_j(s)K_{jb}(s). \end{aligned} \quad (3)$$

For the amplitude $A_{ab}(s)$ one obtains the standard K-matrix expression which in the matrix form reads:

$$\hat{A} = \hat{A}i\hat{\rho}\,\hat{K} + \hat{K}, \quad \text{or} \quad \hat{A} = \hat{K}(I - i\hat{\rho}\,\hat{K})^{-1}. \quad (4)$$

The factor $(I - i\hat{\rho}\,\hat{K})^{-1}$ describes the rescattering of mesons, it is inherent not only in two-meson transition amplitudes but in production amplitudes as well. The P-vector method describes the production of particles in cases when an initial interaction should be taken into account only once, for example, for the production of mesons from the $\gamma\gamma$ collision or from proton-antiproton annihilation:

$$A_k(\bar{p}p) = P_j[(I - i\hat{\rho}\,\hat{K})^{-1}]_{jk}. \quad (5)$$

Elements of the vector P_j have a form similar to the K-matrix elements, Eq. (1):

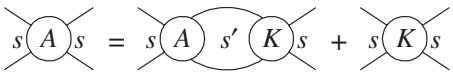

FIG. 2. Graphical representation of the spectral integral equation for the K-matrix amplitude.

$$P_j = \sum_\alpha \frac{\Lambda_\alpha g_j^{(\alpha)}}{M_\alpha^2 - s} + F_j. \tag{6}$$

The first term in Eq. (6) refers to the production of resonances; the second one, F_j, to a nonresonant production.

The standard form of the two-particle phase volume is

$$\rho_a(s, m_{1a}, m_{2a}) = \sqrt{\frac{(s-(m_{1a}+m_{2a})^2)(s-(m_{1a}-m_{2a})^2)}{s^2}}, \quad a = 1,2,3,4, \tag{7}$$

where m_{1a} and m_{2a} are masses of the final particles. In the case of different masses this expression includes the term $\sqrt{s-(m_{1a}-m_{2a})^2}$ which in the K-matrix approach can be a source of false kinematic singularities on the first (physical) sheet: the loop diagram amplitude, $B(s)$, does not contain this type of singularities. Such a cancellation can be taken into account effectively by replacing the $\eta\eta'$ phase volume:

$$\sqrt{\frac{(s-(m_{1a}+m_{2a})^2)(s-(m_{1a}-m_{2a})^2)}{s^2}} \to \sqrt{\frac{s-(m_{1a}+m_{2a})^2}{s}}. \tag{8}$$

For the restoration of the amplitude we need to take into account not only the cuts related to threshold singularities of the stable particles but nonstable ones as well. In the 00^{++} amplitude the four-pion state gives cuts related to $\pi\pi\pi\pi$ (at the real s-axis, $\sqrt{s} = 4m_\pi$) and in the complex-s plane related to the production of vector and scalar particles: $\pi\pi\rho$ (at $\sqrt{s} = 2m_\pi + m_\rho$ with a complex mass m_ρ), $\rho\rho$ (at $\sqrt{s} = 2m_\rho$) and $f_0 f_0$. Let us write the phase space factor for the $\rho\rho$ state which contains 4π, $\pi\pi\rho$ and $\rho\rho$ threshold singularities:

$$\begin{aligned}\rho_{4\pi}(s) = &\int_{4m_\pi^2}^{(\sqrt{s}-2m_\pi)^2} \frac{ds_{12}}{\pi} \\ &\times \int_{4m_\pi^2}^{(\sqrt{s}-\sqrt{s_{12}})^2} \frac{ds_{34}}{\pi} G_{in}^2(s, s_{12}, s_{34}) \rho(s, \sqrt{s_{12}}, \sqrt{s_{34}}) \\ &\times \frac{G^2(s_{12})(s_{12}-4m_\pi^2)\rho(s_{12}, m_\pi, m_\pi)}{(s_{12}-M_\rho^2)^2 + (M_\rho\Gamma_\rho)^2} \\ &\times \frac{G^2(s_{34})(s_{34}-4m_\pi^2)\rho(s_{34}, m_\pi, m_\pi)}{(s_{34}-M_\rho^2)^2 + (M_\rho\Gamma_\rho)^2}.\end{aligned} \tag{9}$$

The form factors $G_{in}(s, s_{12}, s_{34})$, $G(s_{12})$, $G(s_{34})$ are introduced into Eq. (9) to provide the convergency of the integrals. This phase volume describes production of $\rho\rho$ in the S-wave and P-wave production of pions in the ρ-meson decays and was used, for example, in the analysis [9]. As in this analysis $G(s_{ij})$ are parameterized as P-wave Blatt-Weisskopf form factors and $G_{\rm in} = 1$.

Being near a pole, hadronic production cuts split this pole into several ones located on different sheets of the complex-s plane.

B. The D-matrix approach

The considered above approaches allow us to distinguish between ''bare'' and ''dressed'' particles: due to meson rescattering the bare particles, with poles on the real-s axis, are transformed into particles dressed by ''coats'' of meson states. In the K-matrix approach we deal with a ''coat'' formed by real particles—the contribution of virtual ones is included in the principal part of the loop diagram, $B(s)$, and is taken into account effectively by the renormalization of mass and couplings.

In the dispersion relation D-matrix approach one can take into account the coat of virtual mesons. The D-matrix amplitudes describe transitions of bare states.

Let us consider the block $D_{\alpha\beta}$ which describes a transition between the bare state α (but without the propagator of this state) and the bare state β (with the propagator of this state included). For such a block one can write the following equation:

$$D_{\alpha\beta} = D_{\alpha\gamma} \sum_j B_{\gamma\eta}^j d_{\eta\beta} + d_{\alpha\beta}, \tag{10}$$

or, in the matrix form:

$$\hat{D} = \hat{D}\,\hat{B}\,\hat{d} + \hat{d}, \qquad \hat{D} = \hat{d}(I - \hat{B}\,\hat{d})^{-1} \tag{11}$$

Here the $\hat{d}$ is a diagonal matrix of the propagators:

$$\hat{d} = \mathrm{diag}\left(\frac{1}{M_1^2 - s}, \frac{1}{M_2^2 - s}, \ldots, \frac{1}{M_N^2 - s}, R_1, R_2 \ldots\right), \tag{12}$$

where R_α are propagators for nonresonant transitions (discussed below), and the elements of the $\hat{B}$-matrix are equal to

$$\hat{B}_{\alpha\beta} = \sum_j B_{\alpha\beta}^j = \sum_j \int \frac{ds'}{\pi} \frac{g_j^{R(\alpha)} \rho_j(s', m_{1j}, m_{2j}) g_j^{L(\beta)}}{s' - s - i0}. \tag{13}$$

The $g_j^{R(\alpha)}$ and $g_j^{L(\alpha)}$ are right and left vertices for a transition from the bare state α to the channel j. For the pole terms there is a clear factorization:

$$g_j^{R(\alpha)} = g_j^{L(\alpha)} = g_j^{(\alpha)}. \tag{14}$$

However, nonresonant terms do not provide such a factorization. A solution to this problem is to introduce for nonresonant transitions a separate propagator and vertices from every initial state i. Moreover, for the description of the nonresonant terms between different initial and final states a second propagator with permutated left and right vertices is needed. In this case the propagator index provides automatically a unique identification of the transition term. Then for nonresonant transitions from the $\pi\pi$ channel we have

$$g_i^{L(N+1)} R_1 g_j^{R(N+1)} + g_i^{L(N+2)} R_2 g_j^{R(N+2)}, \qquad (15)$$

where N is the number of pole terms. The nonzero left and right vertices can be taken as

$$g_j^{L(N+1)} = f_{1j}\frac{1\,\mathrm{GeV}^2 + s_0}{s + s_0}, \quad g_1^{R(N+1)} = 1,$$
$$R_1 = 1, \quad g_1^{L(N+2)} = 1, \quad g_{j>1}^{R(N+2)} = f_{1j}\frac{1\,\mathrm{GeV}^2 + s_0}{s + s_0},$$
$$R_2 = 1 \text{ and } g_{j>1}^{R(N+1)} = g_{j>1}^{L(N+2)} = g_1^{R(N+2)} = 0. \qquad (16)$$

Another alternative parametrization for the nonzero terms is

$$g_j^{L(N+1)} = f_{1j}, \quad g_1^{R(N+1)} = 1, \quad R_1 = \frac{1\,\mathrm{GeV}^2 + s_0}{s + s_0},$$
$$g_1^{L(N+2)} = 1, \quad g_{j>1}^{R(N+2)} = f_{1j}, \quad R_2 = \frac{1\,\mathrm{GeV}^2 + s_0}{s + s_0}. \qquad (17)$$

With such a definition the amplitude A_{ab} is the convolution of the matrix $D_{\alpha\beta}$ with right and left coupling vectors, $g_a^{(R,\alpha)}$ and $g_b^{(L,\beta)}$:

$$A_{ab} = \sum_{\alpha,\beta} g_a^{R(\alpha)} d_{\alpha\alpha} D_{\alpha\beta} g_b^{L(\beta)}. \qquad (18)$$

The P-vector amplitude has the form:

$$A_b = \sum_{\alpha,\beta} \tilde{P}^{(\alpha)} d_{\alpha\alpha} D_{\alpha\beta} g_b^{L(\beta)},$$
$$\tilde{P} = (\Lambda_1, \Lambda_2, \ldots, \Lambda_n, F_1/R_1 \ldots), \qquad (19)$$

where couplings Λ_α and nonresonant terms F_j are the same as in Eq. (6).

In the present fits we calculate the elements of the $B^j_{\alpha\beta}$ using one subtraction taken at the channel threshold $M_j = (m_{1j} + m_{2j})$:

$$B^j_{\alpha\beta}(s) = B^j_{\alpha\beta}(M_j^2) + (s - M_j^2) \times \int_{m_a^2}^{\infty} \frac{ds'}{\pi} \frac{g_j^{R(\alpha)} \rho_j(s', m_{1j}, m_{2j}) g_j^{L(\beta)}}{(s' - s - i0)(s' - M_j^2)}. \qquad (20)$$

In the case of the nonresonant terms parameterized in the form (17) and the S-wave vertices parameterized as constants the expression for elements of the $\hat{B}$ matrix can be rewritten as

$$B^j_{\alpha\beta}(s) = g_a^{R(\alpha)}\Big(b^j + (s - M_j^2) \times \int_{m_a^2}^{\infty} \frac{ds'}{\pi} \frac{\rho_j(s', m_{1a}, m_{2a})}{(s' - s - i0)(s' - M_j^2)}\Big) g_b^{L(\beta)}, \qquad (21)$$

where the parameters b^j depend on decay channels only.

In the case of the D-matrix approach it is not necessary to introduce the regularization of the $\eta\eta'$ phase volume and, therefore, we use the standard expression (7). It is also not necessary to introduce any regularization for the D-matrix elements at $s = 0$: this point is not singular in this approach. Thus, in the D-matrix fits, the term with the Adler zero was introduced in the $\pi\pi$ channel only. Technically, it can be done either by the modification of vertices or by the modification of the $\pi\pi$ phase volume:

$$\rho_1(s, m_\pi, m_\pi) = \frac{s - s_A}{s + s_{A0}}\sqrt{\frac{s - 4m_\pi}{s}}. \qquad (22)$$

For $q\bar{q}$ states one can relate the decay couplings $g_a^{(\alpha)}$ in terms of the rules of quark combinatorics (see [14] or in more detail in [15]). The couplings for channels $a = \pi\pi$, $K\bar{K}$, $\eta\eta$, $\eta\eta'$, calculated in the leading terms of the $1/N_c$ expansion, are presented in Table I (this Table is given also in [1]). The couplings depend on the constant g which is universal for all nonet states, the mixing angle Φ which determines the proportion of the $n\bar{n} = (u\bar{u} + d\bar{d})/\sqrt{2}$ and $s\bar{s}$ components in the decaying $q\bar{q}$ state, and the $s\bar{s}$ production suppression parameter $\lambda \sim 0.5$–0.7. Two scalar-isoscalar states of the same nonet are orthogonal if

$$\Phi^{(I)} - \Phi^{(II)} = \pm 90°. \qquad (23)$$

The equality of the coupling constants g and the fulfilment of the mixing angle relation (23) is a basis for the determination of mesons of a $q\bar{q}$ nonet.

The gluonic states are decaying in the channels $a = \pi\pi$, $K\bar{K}$, $\eta\eta$, $\eta\eta'$ with the same couplings as the $q\bar{q}$ state but at a fixed mixing angle $\Phi \to \Phi_{\mathrm{glueball}}$ which is determined by the value of λ, namely: $\Phi_{\mathrm{glueball}} = \cos^{-1}\sqrt{2/(2 + \lambda)}$. The corresponding couplings are given in Table I as well.

TABLE I. Coupling constants given by quark combinatorics for $(q\bar{q})_{I=0}$ meson and glueball decays into two pseudoscalar mesons in the leading terms of the $1/N_c$ expansion. The Φ is the mixing angle for $n\bar{n} = (u\bar{u} + d\bar{d})/\sqrt{2}$ and $s\bar{s}$ states: $n\bar{n}\cos\Phi + s\bar{s}\sin\Phi$. The Θ is the mixing angle for $\eta - \eta'$ mesons: $\eta = n\bar{n}\cos\Theta - s\bar{s}\sin\Theta$ and $\eta' = n\bar{n}\sin\Theta + s\bar{s}\cos\Theta$ with $\Theta \simeq 37°$.

Decay channel	$q\bar{q}$-meson decay coupling	gg state decay coupling	Identity factor
$\pi^0\pi^0$	$g\cos\Phi/\sqrt{2}$	G	1/2
$\pi^+\pi^-$	$g\cos\Phi/\sqrt{2}$	G	1
K^+K^-	$g(\sqrt{2}\sin\Phi + \sqrt{\lambda}\cos\Phi)/\sqrt{8}$	$\sqrt{\lambda}G$	1
$K^0\bar{K}^0$	$g(\sqrt{2}\sin\Phi + \sqrt{\lambda}\cos\Phi)/\sqrt{8}$	$\sqrt{\lambda}G$	1
$\eta\eta$	$g(\cos^2\Theta\cos\Phi/\sqrt{2} + \sqrt{\lambda}\sin\Phi\sin^2\Theta)$	$G(\cos^2\Theta + \sqrt{\lambda}\sin^2\Theta)$	1/2
$\eta\eta'$	$g\sin\Theta\cos\Theta(\cos\Phi/\sqrt{2} - \sqrt{\lambda}\sin\Phi)$	$G(1 - \lambda)\cos\Theta\sin\Theta$	1

III. CONFINEMENT INTERACTION IN THE $q\bar{q}$ SECTOR

The description of mesons of the $q\bar{q}$ sector is a source of information about quark confinement interaction. These interactions contain t-channel singularities of scalar and vector type. The t-channel exchange interaction can be both in white and color states, $\mathbf{c} = \mathbf{1} + \mathbf{8}$ though, of course, the color-octet interaction plays a dominant role in meson formation.

The observed linearity of the $q\bar{q}$-meson trajectories in the (n, M^2) planes [29], where n is the radial quantum number of the $q\bar{q}$ meson with mass M, provides us the t-channel singularity $V_{\rm conf} \sim 1/q^4$ or, in coordinate representation, $V_{\rm conf} \sim r$. In the coordinate representation the confinement interaction can be written in the following potential form [15,24]:

$$V_{\rm conf} = (I \otimes I) b_S r + (\gamma_\mu \otimes \gamma_\mu) b_V r, \qquad b_S \simeq -b_V \simeq 0.15\ \text{GeV}^{-2}. \tag{24}$$

The first term in (24) refers to scalar interaction $(I \otimes I)$, the second one to vector $(\gamma_\mu \otimes \gamma_\mu)$—in the $q\bar{q}$ sector the scalar and vector forces are approximately equal.

White remnants of the confinement singularities

We have serious reasons to suspect that the confinement singularities (the t-channel singularities in the scalar and vector states) have a complicated structure. In the color space these are octet states but, may be, they contain also white components. The octet exchange interaction contains quark-antiquark and gluonic blocks. Therefore, the question is whether $V^{(1)}_{\rm confinement}(q^2)$ has the same singular behavior as $V^{(8)}_{\rm confinement}(q^2)$. The observed linearity of the (n, M^2) trajectories, up to the large-mass region, $M \sim$ 2000–2500 MeV [29], favors the idea of the universality in the behavior of potentials $V^{(1)}_{\rm confinement}$ and $V^{(8)}_{\rm confinement}$ at large r, or small q. To see that, let us consider, as an example, the process $\gamma^* \to q\bar{q}$, Fig. 3(a). We discuss the color neutralization mechanism of outgoing quarks as a breaking of the gluonic string by newly born $q\bar{q}$ pairs, see the discussion in [30]. At large distances, which correspond to the formation of states with large masses, several new $q\bar{q}$ pairs should be formed. It is natural to suggest that a convolution of the quark-gluon combs governs the interaction forces of quarks at large distances, see Fig. 3(b). The mechanism of the formation of new $q\bar{q}$ pairs to neutralize color charges does not have a selected color component. In this case all color components $3 \otimes \bar{3} = 1 + 8$ behave similarly, that is, at small q^2 the singlet and octet components of the potential are uniformly singular, $V^{(1)}_{\rm confinement}(q^2) \sim V^{(8)}_{\rm confinement}(q^2) \sim 1/q^4$.

If the confinement singularities have, indeed, white constituents, this raises immediately the following questions:

(i) How do these constituents reveal themselves in white channels?

(ii) Can they be identified?

In the scalar channel we face the problem of the σ meson $(IJ^{PC} = 00^{++})$: what is the nature of this state? If the white scalar confinement singularity exists, it would be reasonable to consider it as the σ meson revealing itself: because of the transitions into the $\pi\pi$ state, the confinement singularity could move to the second sheet. If so, the σ meson can certainly not reveal itself as a lonely amplitude singularity $1/t^2$ but a standard amplitude pole or a group of poles.

A similar scenario may be valid also for the vector confinement singularity in the $\pi\pi\pi$ $(IJ^{PC} = 01^{--})$ channel. In this case it is natural to assume that the white confinement singularity couples with the channel $\rho\pi$, splits and dives into the complex-$M_{\pi\pi\pi}$ plane.

An illustrative example of a set of loop diagrams of the Fig. 3(c) type is considered in Appendix A. In this example we demonstrate how the strong singularity, $1/t^2$, may arise in scalar and vector channels of the interaction block. An example of the simple parametrization of this singularity is given in Appendix B.

IV. THE K-MATRIX AND D-MATRIX APPROACHES IN FITS TO THE DATA AT $0.28 \le \sqrt{s} \le 1.95$ GEV

Here we present a comparative analysis of the results obtained with the K-matrix and D-matrix methods. These approaches give rather similar results for the f_0 resonances at $\sqrt{s} \le 2$ GeV. In Table II we show the data used in these analyses and give corresponding χ^2 for

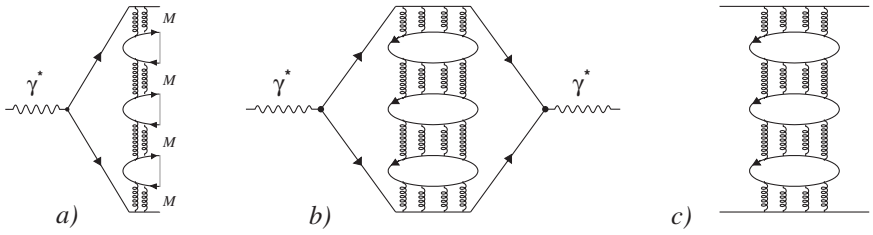

FIG. 3. (a) Quark-gluonic comb produced by breaking a string by quarks flowing out in the process $e^+e^- \to \gamma^* \to q\bar{q} \to$ mesons. (b) Convolution of the quark-gluonic combs. (c) Example of diagrams describing interaction forces in the $q\bar{q}$ systems.

TABLE II. List of the reactions and χ^2 values for the K-matrix and D-matrix solutions: Solutions 3, 5 with taken into account confinement interaction, solutions 1, 2, 4 without it.

	Sol. 1 K-matrix 0	Sol. 2 D-matrix 0	Sol. 3 D-matrix $\sim 1/s^2$	Sol. 4 D-matrix 0	Sol. 5 D-matrix $\sim 1/s^2$	N of points
			The Crystal Barrel data			
From liquid H_2:						
$\bar{p}p \to \pi^0\pi^0\pi^0$	1.32	1.37	1.39	1.44	1.45	7110
$\bar{p}p \to \pi^0\eta\eta$	1.33	1.34	1.34	1.33	1.33	3595
$\bar{p}p \to \pi^0\pi^0\eta$	1.24	1.33	1.33	1.55	1.55	3475
From gaseous H_2:						
$\bar{p}p \to \pi^0\pi^0\pi^0$	1.39	1.44	1.45	1.48	1.49	4891
$\bar{p}p \to \pi^0\eta\eta$	1.31	1.34	1.30	1.43	1.31	1182
$\bar{p}p \to \pi^0\pi^0\eta$	1.20	1.22	1.22	1.31	1.32	3631
From liquid H_2:						
$\bar{p}p \to \pi^+\pi^0\pi^-$	1.54	1.46	1.45	1.46	1.47	1334
From liquid D_2:						
$\bar{p}n \to \pi^0\pi^0\pi^-$	1.51	1.47	1.47	1.46	1.46	825
$\bar{p}n \to \pi^-\pi^-\pi^+$	1.61	1.54	1.55	1.50	1.51	823
From liquid H_2:						
$\bar{p}p \to K_S K_S \pi^0$	1.09	1.10	1.10	1.10	1.10	394
$\bar{p}n \to K^+K^-\pi^0$	0.98	1.00	1.00	1.03	1.02	521
$\bar{p}n \to K_L K^\pm \pi^\mp$	0.78	0.79	0.79	0.79	0.79	737
From liquid D_2:						
$\bar{p}p \to K_S K_S \pi^-$	1.66	1.64	1.64	1.64	1.63	396
$\bar{p}n \to K_S K^-\pi^0$	1.33	1.31	1.31	1.31	1.31	378
			The GAMS data			
$\pi\pi \to (\pi^0\pi^0)_{S\text{-wave}}$	1.23	1.13	1.15	1.32	1.30	68
$\pi\pi \to (\eta\eta)_{S\text{-wave}}$	1.02	1.05	1.03	1.58	1.43	15
$\pi\pi \to (\eta\eta')_{S\text{-wave}}$	0.45	0.30	0.35	0.35	0.34	9
			The BNL data			
$\pi\pi \to (K\bar{K})_{S\text{-wave}}$	1.32	1.13	1.14	0.97	1.07	35
			The CERN-Munich data: $Y_0^0 \ldots Y_6^1$			
$\pi^-\pi^+ \to \pi^-\pi^+$	1.82	1.86	1.86	2.05	2.03	705
			The K_{e4} decay data			
$\delta_0^0(\pi^-\pi^+ \to \pi^-\pi^+)$	1.51	1.02	0.84	0.80	0.83	17

different fits. In Table III we list the masses of bare states, mixing angles and other parameters used in the minimization procedure.

A. The K-matrix fit

In the analysis of the present data set we fitted data in two steps. In the first step all couplings were optimized as free parameters; in the second step we imposed relations Table I for the poles with masses above 1 GeV. We did not observe any deterioration of the data description due to these restrictions but a rather notable improvement in the convergency of the fits. For the lowest K-matrix pole we do not impose any constraints: the global coupling and mixing angle for this pole given in Table III are simply calculated from the couplings into the $\pi\pi$ and $K\bar{K}$ channels.

In the present solutions there are two candidates for a glueball: it is either the third or the fourth K-matrix pole (with a mass around 1200 MeV). For the glueball candidate we introduced in addition a glueball decay coupling (see Table I). However, this coupling provided only a small improvement and did not allow us to distinguish between these two cases.

The fit is hardly sensitive to the $\pi\pi\pi\pi$ couplings for the two lowest K-matrix poles; in the final solution we fix them to be zero.

To get a combined description of all reactions, we introduced nonresonant terms for the transition from the $\pi\pi$ channel to other final states. We did not find a notable sensitivity to nonresonant transitions between other channels. In the paper [31] a more sophisticated nonresonant behavior was suggested. The exchange of the $\rho(770)$ and $f_2(1270)$ states was introduced to fix the isotensor

TABLE III. The f_0^{bare} resonances: masses M_n (in MeV units), decay coupling constants g_n (in GeV units, $g_{4\pi} \equiv g_5$), mixing angles (in degrees) defined as in Table I, background terms f_n and confinement singularity term G/s^2 (factor G in GeV units). In all fits the position of the Adler zero was fixed at $s_A = 0.5m_\pi^2$.

	Sol. 1	Sol. 2	Sol. 3	Sol. 4	Sol. 5
M_1	671	685	697	611	615
M_2	1205	1135	1135	1078	1096
M_3	1560	1561	1558	1575	1572
M_4	1210	1290	1284	1334	1330
M_5	1816	1850	1848	1858	1857
g_1	0.860	0.926	0.892	1.090	1.083
g_2	0.956	0.950	0.935	0.099	1.066
g_3	0.373	0.290	0.284	0.302	0.302
g_4	0.447	0.307	0.308	0.264	0.275
g_5	0.458	0.369	0.370	0.317	0.330
$g^{(1)}_{\eta\eta}$	−0.382	−0.213	−0.232	−0.176	−0.193
$g^{(1)}_{\eta\eta'}$	−0.322	−0.500	−0.500	−0.500	−0.500
$g^{(1)}_{4\pi}$, $g^{(2)}_{4\pi}$	0	0	0	0	0
$g^{(3)}_{4\pi}$	0.638	0.534	0.530	0.511	0.514
$g^{(4)}_{4\pi}$	0.997	0.790	0.794	0.691	0.702
$g^{(5)}_{4\pi}$	−0.901	−0.862	−0.856	−0.797	−0.814
Φ_1	−74	−83	−82	−81	−82
Φ_2	6	−2.6	−1.9	−1.1	−2.4
Φ_3	9	5	5	5	5
Φ_4	38	31	32	25	25
Φ_5	−64	−71	−68	−77	−77
$f_{\pi\pi\to\pi\pi}$	0.337	0.408	0.358	0.763	0.687
$f_{\pi\pi\to K\bar{K}}$	0.212	0.036	0.044	0.103	0.065
$f_{\pi\pi\to 4\pi}$	−0.199	−0.101	−0.092	−0.051	−0.062
$f_{\pi\pi\to\eta\eta}$	0.389	0.438	0.413	0.538	0.512
$f_{\pi\pi\to\eta\eta'}$	0.394	0.518	0.485	0.610	0.597
G/s^2	0	0	$-0.00077/s^2$	0	$-0.00071/s^2$

component of the $\pi\pi$ scattering. In the isoscalar sector these exchanges were combined with a K-matrix part by the Dalitz-Tuan approach. However, for the scalar sector such a parametrization produced a very similar result as a K-matrix approach with a constant nonresonant contribution.

The K_{e4} data can be described with a very small re-optimization of the K-matrix parameters found in [12–14]. We did not find any change in the pole structure of the scalar-isoscalar amplitude above 900 MeV. However, one of the pole singularities situated around $s = 0$ moved to higher masses. Its position, as well as the positions of other poles, is given below in Table IV.

B. The D-matrix fits

D-matrix parameters can be expressed in the same terms (bare masses and couplings) as parameters of a K-matrix fit. The subtraction point for calculation of the real part of the loop diagrams, i.e. $B^j_{\alpha\beta}(M_s^2)$ in Eq. (21), was taken at the corresponding two-particle threshold; the

TABLE IV. The positions of the amplitude poles.

	Sol. 1	Sol. 2	Sol. 3	Sol. 4	Sol. 5
σ meson	420-i 395	407-i 281	365-i 283	414-i 186	406-i 192
$f_0(980)$	1014-i 31	1015-i 36	1012-i 31	1005-i 20	1005-i 23
$f_0(1300)$	1302-i 180	1307-i 137	1303-i 140	1332-i 140	1326-i 137
$f_0(1500)$	1487-i 58	1487-i 60	1483-i 55	1487-i 55	1486-i 55
$f_0(1750)$	1738-i 152	1781-i 140	1787-i 143	1795-i 109	1794-i 114

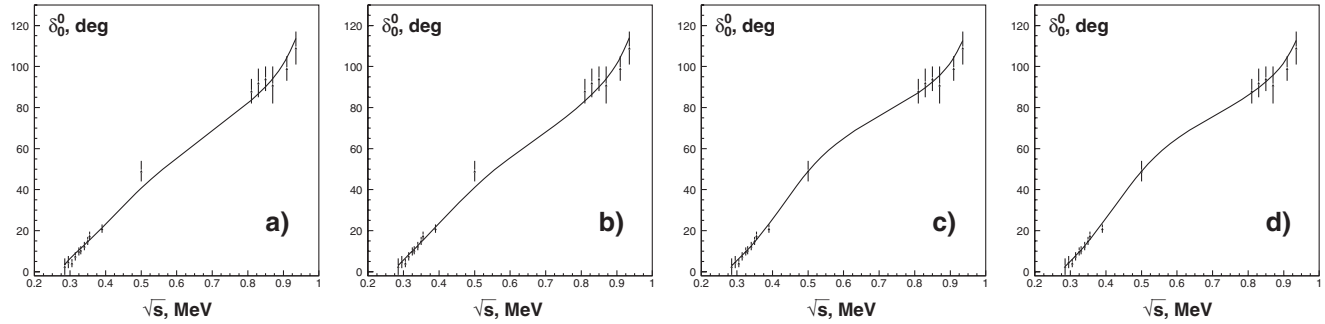

FIG. 4. Description of the K_{e4} data with the D-matrix solutions 2, 3 (a, b) (with standard errors for the point $\delta_0^0(500\ \text{MeV})$ extracted from the $K \to \pi\pi$ data [32]) and solutions 4, 5 (c, d) (with the decreased error for this point).

parameters b^j were optimized in the fit. In such an approach our data base can be described with a very similar quality as in the framework of the K-matrix approach, see Table II.

As expected, the D-matrix fit provides a better description of the K_{e4} data due to the more correct behavior of the amplitude near left-hand side singularities. The behavior of the phase shift δ_0^0 and its description in the mass region from the threshold to 1 GeV is shown in Fig. 4.

Below we present four D-matrix solutions: the bare masses and their couplings are given in Table III (Solutions 2,3,4,5). In Solutions 2,3 the $K \to \pi\pi$ point near 500 MeV [32] was taken with the error given by the experimental group. However, these solutions do not reproduce this point satisfactory. To force the $\pi\pi$ phase shift to describe this point, we decreased the error by a factor 10 and repeated the D-matrix fit of the data. In such an approach we were able to describe the data at 500 MeV rather well (Solutions 4,5); however, we obtained a systematically worse description of the proton-antiproton annihilation into the $\pi^0\pi^0\pi^0$ and $\eta\eta\pi^0$ channels (see Table II). The data point was criticized in a number of papers and the reanalysis [33] produced a result which is lower by about 5 degrees. However, the KLOE Collaboration did not publish any revision of this point and we would like to investigate its influence on the position of the lowest pole and scattering length parameter. The solution with the $1/s^2$ term included (Solutions 3,5) produced a better total χ^2 and a slightly better description of the K_{e4} data. The term $1/s^2$ can produce two additional poles in the mass region below the $\pi\pi$ threshold. The pole in the mass region around 400 MeV has moved to lower masses by about 80 MeV compared to solutions without the $1/s^2$ term, see Table IV, while the poles situated above 900 MeV practically do not change their positions.

Examples of the description of experimental Dalitz plots with our D-matrix solution (Solution 2) for proton-antiproton annihilation into three meson states are shown in Figs. 3 and 6. Mass and angular distributions for selected Dalitz plots are given in Figs. 7–9. The description of the CERN-Munich data [8] is shown in Fig. 10 and the description of the S-wave intensities for $\pi\pi$ transition into different final states in Fig. 11.

It is seen from Table III that the masses of bare states are hardly changed from the K-matrix solution and most of the couplings are shifted by less than 20%. The positions of the amplitude poles above 900 MeV also changed very little, see Table IV.

The relative position of the poles and the threshold singularity cuts is demonstrated in Fig. 1.

We see that a fit of the K_{e4} data with the use of the D-matrix approach unambiguously reveals the pole in the mass region around 300–400 MeV, the low-mass σ meson.

To trace the origin of the σ pole, we multiplied all couplings by the factor β and the nonresonant terms by β^2, and scanned this parameter from 1 (the physical amplitude) to 0 (amplitude with poles corresponding to the bare masses). Such an investigation shows that the σ pole is originated from the Adler regularization term. In the best fit the Adler regularization point is optimized rather close to the physical region $s_{A0} \simeq 0.15\ \text{GeV}^2$. To check the stability of this point we have performed the fit with this point fixed at $s_{A0} = 0.5$ $s_{A0} = 1$ and $s_{A0} = 1.5\ \text{GeV}^2$. We observe a small deterioration of the total χ^2 due to a worse description of the $\pi\pi \to K\bar{K}$ and $\pi\pi \to \eta\eta$ amplitudes. However, the fit with $s_{A0} = 0.5\ \text{GeV}^2$ gives the best description for the proton-antiproton annihilation into the $\pi^0\pi^0\pi^0$ channel that is one of the most sensitive reactions to the description of the low $\pi\pi$ mass region. The positions of the poles in all three solutions coincide remarkably well and hence, we conclude that the position of the σ meson depends very little on the exact position of the Adler regularization term.

C. Calculation of the scattering length

In our expression for the $\pi\pi$ scattering amplitude which takes into account the $\pi^0\pi^0$ and $\pi^+\pi^-$ phase volumes the $\pi\pi$ phase does not go to zero on the threshold of two charged pions, see Appendix C. We calculate the scattering length of the $\pi^+\pi^-$ system at the threshold of two charged pions using the following expression:

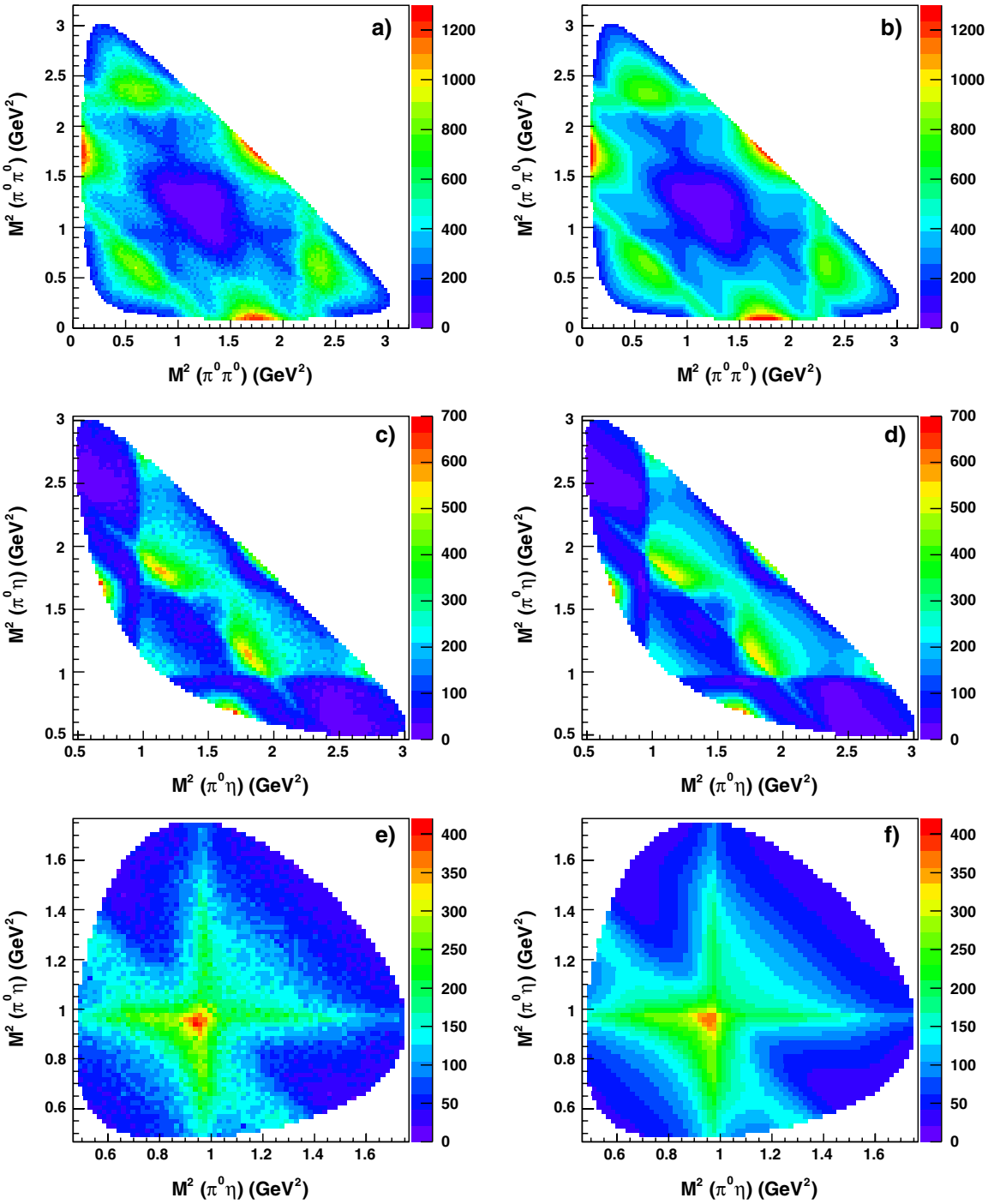

FIG. 5 (color online). Description of the $\bar{p}p$ annihilation in liquid hydrogen into the $3\pi^0$ (a,b), $2\pi^0$ (c,d) and $\pi^0 2\eta$ (e,f) final states. Left-side panels show the experimental Dalitz plots and right-side panels the results of our fit.

$$\frac{\sqrt{s}}{m_{\pi^+}+m_{\pi^-}}\mathrm{Re}[\sin\delta_0^{(0)}e^{i\delta_0^{(0)}}]_{k\to 0}\simeq c_0^{(\pm)}+a_0^{(\pm)}k+b_0^{(\pm)}k^3,$$
$$a_0=\frac{3}{2}a_0^{(\pm)},\quad k=\frac{1}{2}\sqrt{s-(m_{\pi^+}+m_{\pi^-})^2},\quad m_{\pi^+}=m_{\pi^-}. \quad (25)$$

The scattering length values extracted from the D-matrix solutions are equal to

Solution 2	Solution 3	Solution 4	Solution 5
$0.253 m_\pi^{-1}$	$0.209 m_\pi^{-1}$	$0.204 m_\pi^{-1}$	$0.177 m_\pi^{-1}$.

(26)

It is seen that the inclusion of the $1/s^2$ term decreases the scattering length by $\sim 0.05\ m_\pi^{-1}$ and a similar effect comes from a precise description of the $K \to \pi\pi$ experimental point at 500 MeV.

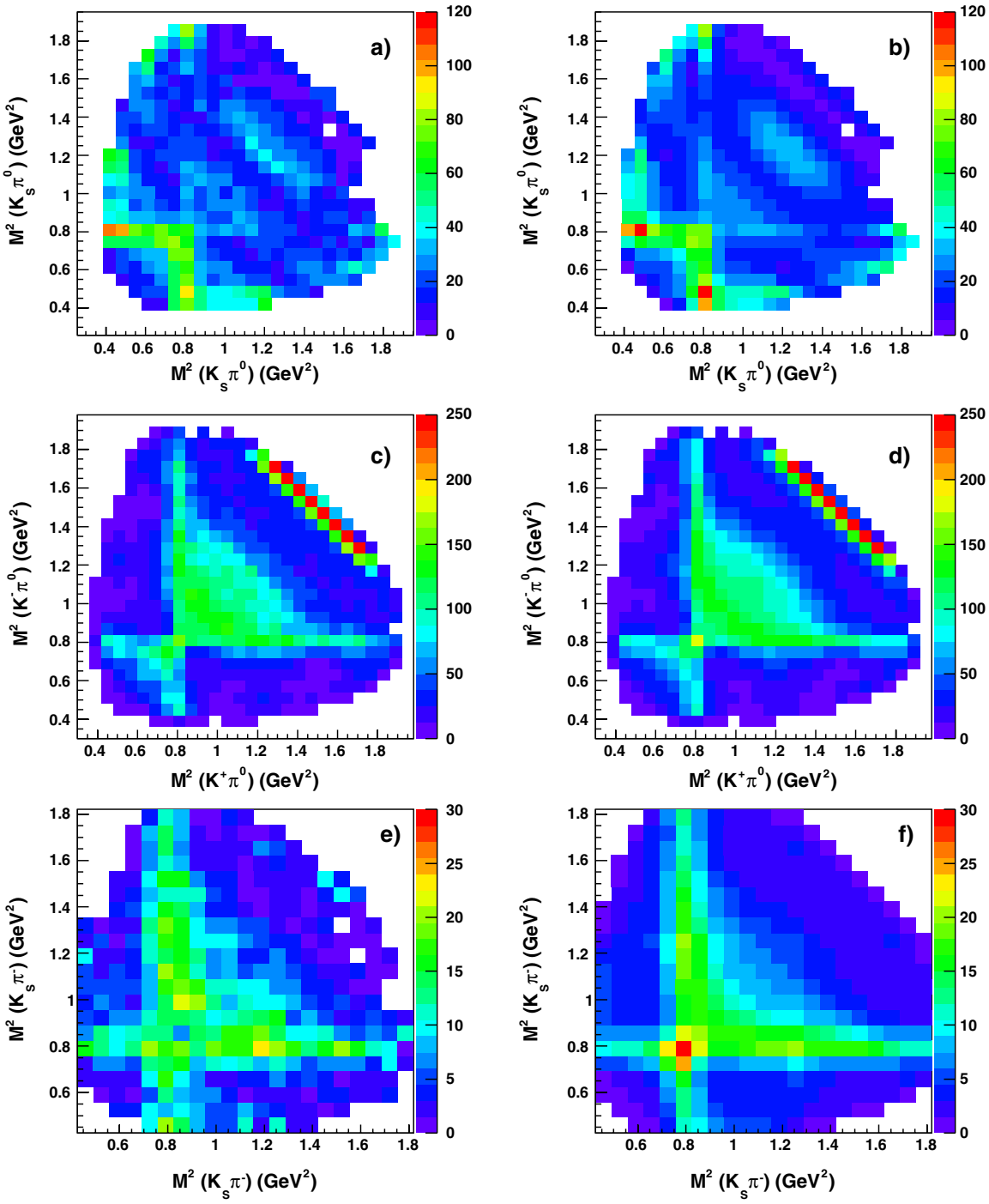

FIG. 6 (color online). Description of the $\bar{p}p$ annihilation in liquid hydrogen into the $K_S K_S \pi^0$ (a,b), $K^+ K^- \pi^0$ (c,d) and in liquid deuterium into $K_S K_S \pi^0$ (e,f) final states. Left-side panels show the experimental Dalitz plots and right-side panels the results of our fit.

The amplitude phase was extracted by the K_{e4} collaboration under the assumption that it is equal to zero at the threshold of two charged pions. Then there is a question about the uncertainty which appears when these data are fitted with an expression which takes into account exactly the thresholds of neutral and charged pions. To check this we put in Solution 2 all pion masses equal to the mass of a charged pion. As expected, notable deteriorations were observed only in the proton-antiproton annihilation into three neutral pions and at low-energy points for the K_{e4} data. With a very small tuning of the parameters we obtained very similar χ^2 values for the description of the K_{e4} data. The scattering length which in this case is calculated as $a_0 = \frac{3}{2} a_0^{(\pm)}$ appeared to be 0.248 m_π^{-1}. Then,

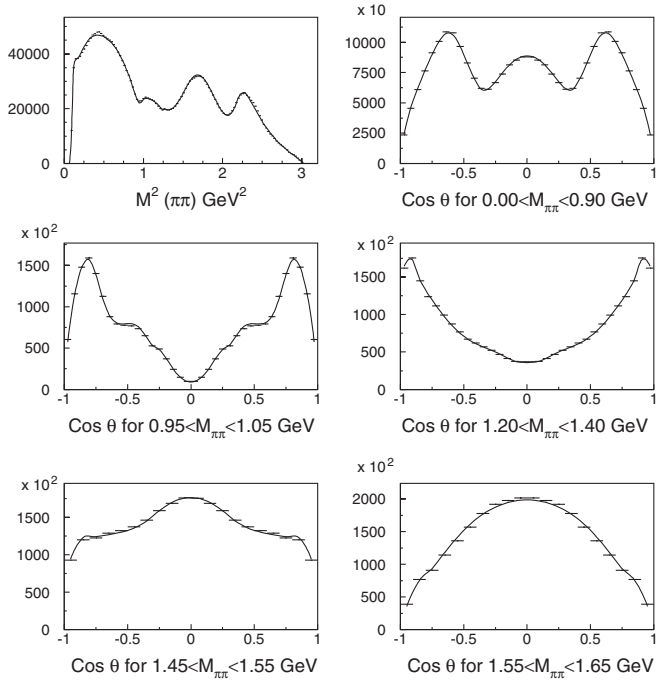

FIG. 7. Mass projections and angular distributions for $\bar{p}p \to 3\pi^0$ (liquid hydrogen target). Experimental data are given as points with error bars and full curves corresponds to Solution 2. Angular distributions are calculated as angular distributions of the spectator particle in the rest frame of given mass slice.

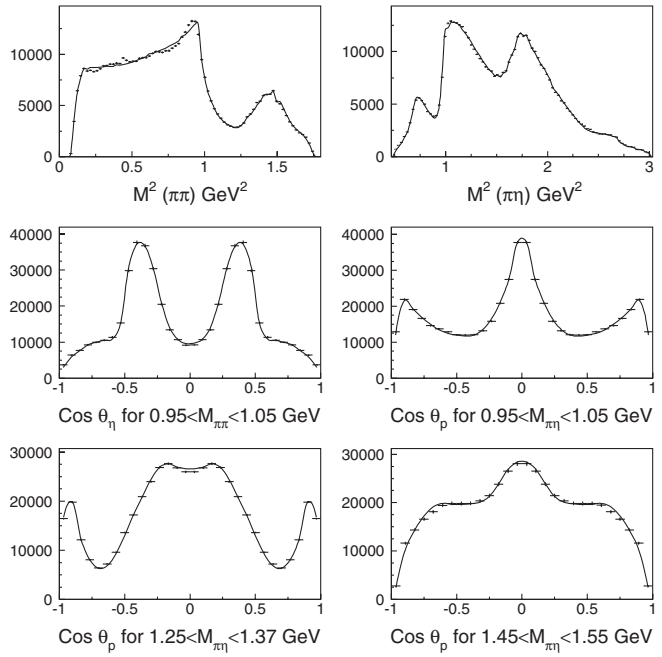

FIG. 8. Mass projections and angular distributions for $\bar{p}p \to 2\pi^0\eta$ (liquid hydrogen target). Experimental data are given as points with error bars and full curves corresponds to Solution 2. Angular distributions are calculated as angular distributions of the spectator particle in the rest frame of given mass slice.

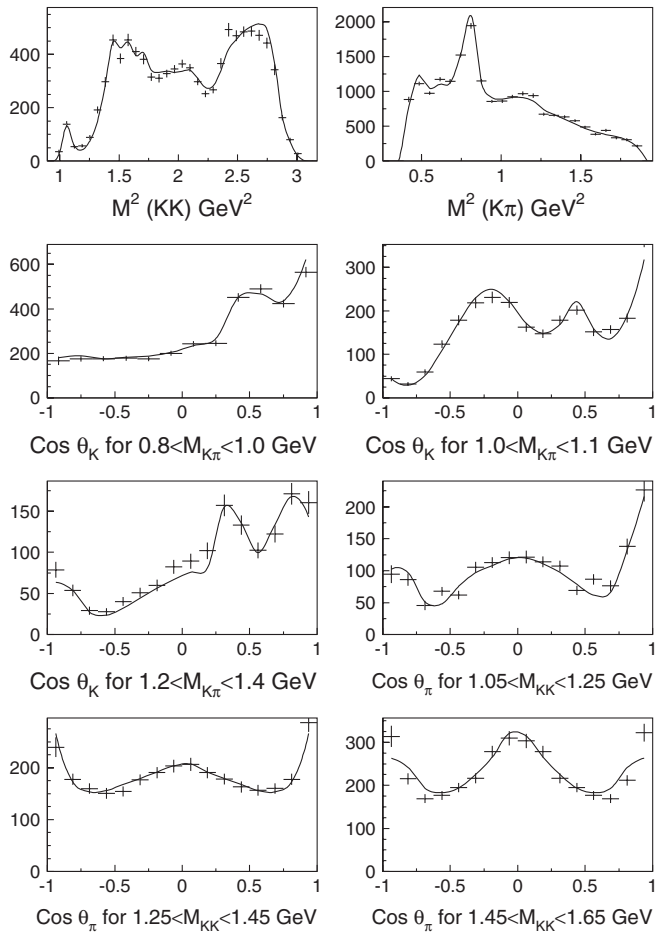

FIG. 9. Mass and angular projections for $\bar{p}p \to K_S K_S \pi^0$ (liquid hydrogen target). Experimental data are given as points with error bars and full curves corresponds to Solution 2. Angular distributions are calculated as angular distributions of the spectator particle in the rest frame of the given mass slice.

with this parameters fixed, we introduced back the difference between neutral and charged pion thresholds but not refitted the data. The scattering length obtained by Eq. (25) was found to be 0.260 m_π^{-1}: a value which is very close to that obtained in Solution 2. Thus, we conclude that the investigated uncertainty is less than 0.010 m_π^{-1} and is smaller than the systematic error which comes from different parameterizations of the amplitude.

It is instructive to compare the results of Eq. (26) with those obtained without taking into account different values of $\pi^0\pi^0$ and $\pi^+\pi^-$ threshold singularities: $a_0 = (0.233 \pm 0.013)m_\pi^{-1}$ [3], $a_0 = (0.220 \pm 0.005)m_\pi^{-1}$ [34].

V. CONCLUSION

The analysis of the large data sets performed in the framework of the K-matrix and D-matrix approaches demonstrates a very good stability for the amplitude parameters and pole positions above 900 MeV. It is seen that in this region the result obtained in the framework of the K-matrix

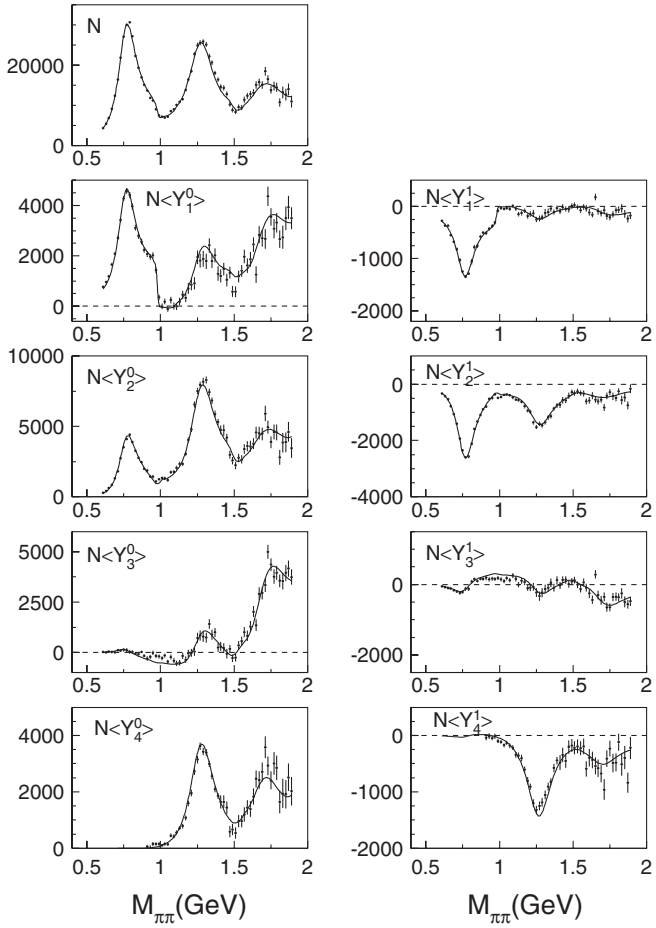

FIG. 10. Description of the CERN-Munich data with the solution 2.

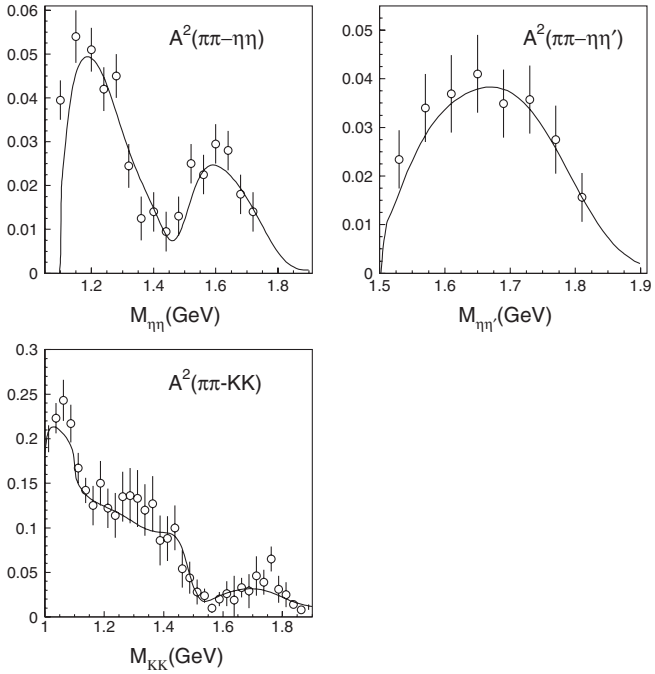

FIG. 11. Description of the S-wave intensities for $\pi\pi \to \eta\eta$, $\pi\pi \to \eta\eta'$ (GAMS) and $\pi\pi \to K\bar{K}$ (BNL) with the solution 2.

approach is affected only slightly if dispersion corrections are taken explicitly into account.

The description of the K_{e4} data demands the presence of the pole slightly above the $\pi\pi$ threshold already in the K-matrix fit. As expected, the effect of the dispersion corrections is the biggest in this mass region. The pole position in D-matrix approach was found to be at $385 \pm 25 - i280 \pm 15$ MeV and the scattering length $0.230 \pm 0.025 m_\pi^{-1}$ in the fits with a systematically lower description of the $K \to \pi\pi$ point. If the fit is enforced to fit this point than the imaginary part of the sigma pole position moves down to $410 \pm 15 - i190 \pm 15$ and the scattering length to $190 \pm 0.020 m_\pi^{-1}$.

The confinement singularity, $\frac{1}{s^2}$, slightly improves the overall description but is not crucial for a good description of the K_{e4} data and for the existence of the σ meson pole singularity. The presence of such a term influences the scattering length, shifting it to lower values (by $\sim 0.05 m_\pi^{-1}$).

The imaginary part of the σ pole position in the solutions which fit precisely the $K \to \pi\pi$ data at 500 MeV is lower by about 100 MeV compare to the solutions where the fit is not forced to describe this point. The scattering length in such solutions is also systematically shifted to lower values by $\sim 0.05 m_\pi^{-1}$.

Within the description of the 00^{++} wave in the channels $\pi\pi$, $\pi\pi\pi\pi$, $K\bar{K}$, $\eta\eta'$ we obtain the following complex masses of the f_0 resonances:

$$
\begin{aligned}
f_0(980) \qquad & M_I = 1011 \pm 5 - i31 \pm 4 \text{ MeV} \\
& M_{II} = 1035 \pm 50 - i460 \pm 50 \text{ MeV} \\
f_0(1300) \qquad & M = 1285 \pm 30 - i160 \pm 20 \text{ MeV} \\
f_0(1500) \qquad & M = 1488 \pm 4 - i53 \pm 5 \text{ MeV} \\
f_0(1790) \qquad & M = 1775 \pm 25 - i140 \pm 15 \text{ MeV}. \qquad (27)
\end{aligned}
$$

The masses of the D-matrix approach, Eq. (27), coincide well with those obtained in the K-matrix approximation [15]. The $f_0(980)$ is determined by two poles, on the second (under the $\pi\pi$ threshold) and third (under the $\pi\pi$ and $K\bar{K}$ thresholds) sheets—the same splitting of poles we have in the K-matrix solutions [35].

For the low-mass region the solution with $1/s^2$ singularity gives several poles on the second sheet:

$$
\begin{aligned}
f_0(\sigma_I) \qquad & M = 365 \pm 15 - i283 \pm 12 \text{ MeV} \\
f_0(\sigma_{II}) \qquad & M = 80 \pm 10 - i187 \pm 15 \text{ MeV} \\
f_0(\sigma_{III}) \qquad & M = -94 \pm 12 - i93 \pm 10 \text{ MeV}. \qquad (28)
\end{aligned}
$$

If the fit is forced to describe the $K \to \pi\pi$ experimental point at 500 MeV, we have

$$f_0(\sigma_I) \qquad M = 406 \pm 15 - i192 \pm 15 \text{ MeV}$$
$$f_0(\sigma_{II}) \qquad M = 74 \pm 10 - i190 \pm 50 \text{ MeV}$$
$$f_0(\sigma_{III}) \qquad M = -96 \pm 22 - i100 \pm 25 \text{ MeV}. \qquad (29)$$

We also test the changes in the description of data with an elimination of the $1/s^2$ singularity. In this case the fit to the data gives the masses of the f_0 resonances at $\sqrt{s} >$ 900 MeV practically the same as in ref. (27)—the changes are in the low-mass pole structure. Without the $1/s^2$ singularity, the position of the σ pole in the fit, neglecting the 500 MeV point, gives

$$f_0(\sigma_I) \qquad M = 407 \pm 12 - i289 \pm 10 \text{ MeV} \qquad (30)$$

and with the fit forced to describe the 500 MeV point:

$$f_0(\sigma_I) \qquad M = 412 \pm 12 - i186 \pm 15 \text{ MeV} \qquad (31)$$

So, the σ meson arises as a pole near the $\pi\pi$ threshold in both versions, with and without including the confinement singularity $(1/s^2)$ into the $\pi\pi$ scattering block. Though the confinement singularity leads to the appearance of several poles under the $\pi\pi$ cut, it is hardly possible to distinguish these two versions on the basis of the data.

ACKNOWLEDGMENTS

This paper was partially supported by the Federal Program of the Russian State under Grant No. RSGSS-3628.2008.2.

APPENDIX A: EXAMPLES OF SETS OF DIAGRAMS RESULTING IN $1/t^2$ SINGULARITIES

Here we consider, as an example, the confinement set of the loop diagrams, Fig. 3(c), and present an illustrative calculation which results in singularities of the $1/t^2$ type in scalar and vector channels. We use the following interaction blocks, see Fig. 12(a):

$$\sum_n \Psi_{\text{meson}(n)}\Psi^*_{\text{meson}(n)} \to G_S^{(L)}((k_1-k_2)^2)\psi(k_1)\bar\psi(k_2) \times G_S^{(R)}((k_1'-k_2')^2)\psi(k_1')\bar\psi(k_2')$$
$$+ G_V^{(L)}((k_1-k_2)^2)\psi(k_1)\gamma_\mu\bar\psi(k_2) \times G_V^{(R)}((k_1'-k_2')^2)\psi(k_1')\gamma_\mu\bar\psi(k_2'). \qquad (A1)$$

Then the confinement interaction turns into a set of the loop diagrams, Figs. 12(b) and 12(c). The scalar and vector exchanges, correspondingly, read:

$$V_S(t) = \frac{B_S(t)}{1-B_S(t)}, \quad V_{V;\mu\nu}(t) = -\delta^\perp_{\mu\nu}\frac{B_V(t)}{1-B_V(t)}. \qquad (A2)$$

For a scalar loop diagram one has

$$B_S(t) = \int_{4m^2}^\infty \frac{dt'}{\pi} d\Phi_2(P';k_1',-k_2')\frac{N_S(t')Sp[(\hat k_2'-m)(\hat k_1'+m)]}{t'-t-i0},$$
$$d\Phi_2(P';k_1',-k_2') = \frac{1}{2(2\pi)^2}d^4k_1'd^4k_2'\delta(k_1'^2-m^2)\delta(k_2'^2-m^2) \to \frac{1}{16\pi}\sqrt{1-\frac{4m^2}{t'}}, \quad Sp[(\hat k_2'-m)(\hat k_1'+m)] \to 2(t'-4m^2). \qquad (A3)$$

Here we replace $G_S^{(R)}G_S^{(L)} \to N_S$. An analogous loop for vector exchange reads:

$$-\delta^\perp_{\mu\nu}B_V(t) = \int_{4m^2}^\infty \frac{dt'}{\pi} d\Phi_2(P';k_1',-k_2')\frac{N_V(t')Sp[\gamma^\perp_\mu(\hat k_2'-m)\gamma^\perp_\nu(\hat k_1'+m)]}{t'-t-i0}$$
$$= -\delta^\perp_{\mu\nu}\int_{4m^2}^\infty \frac{dt'}{\pi}\frac{G_V^2(t')(2m^2+t')}{t'-t-i0}\frac{1}{16\pi}\sqrt{1-\frac{4m^2}{t'}} \qquad (A4)$$

Confinement singularities appear if $B_S(t)$ and $B_V(t)$ behave near $t = 0$ as follows:

$$B_S(t) = 1-\frac{t^2}{\beta_S}+O(t^3), \quad B_V(t) = 1-\frac{t^2}{\beta_V}+O(t^3), \qquad (A5)$$

which means the requirements

$$\frac{d}{dt}B_S(t)|_{t=0} = 0, \qquad \frac{d}{dt}B_V(t)|_{t=0} = 0. \qquad (A6)$$

APPENDIX B: SIMPLIFIED CONSIDERATION OF THE 00^{++} WAVE IN THE LOW-ENERGY REGION

The partial pion-pion scattering amplitude being a function of the invariant energy squared, $s = M^2$, can be represented as a ratio $N(s)/D(s)$ [36], where $N(s)$ has a left-hand cut due to the "forces" (the interactions caused by the t- and u-channel exchanges), and the function $D(s)$ is determined by the rescattering in the s channel. The

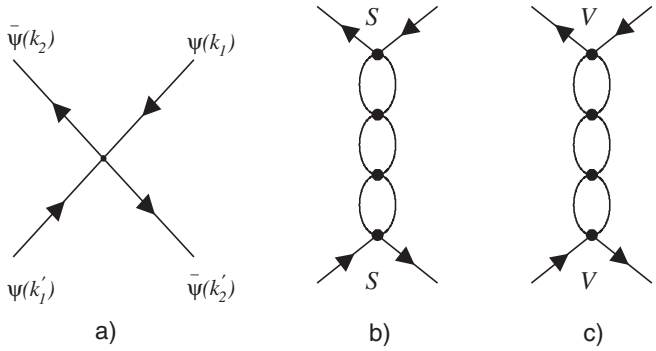

FIG. 12. Interaction block (a) and sets of loop diagrams for S and V exchanges.

standard presentation of the N/D method may be found, for example, in [37].

The $\pi\pi$ scattering block related to the $1/s^2$ singularity reads:

$$G(s)\frac{1}{s^2}G(s). \tag{B1}$$

The s-channel rescattering gives a set of divergent terms which convolutes into the following unitary amplitude:

$$A(s) = G(s)\frac{1}{s^2}G(s) + G(s)\frac{1}{s^2}\Pi(s)\frac{1}{s^2}G(s) + \ldots = \frac{G^2(s)}{s^2 - \Pi(s)} = G^2(s)\left[s^2 - \int_{4m_\pi^2}^{\infty}\frac{ds'}{\pi}\frac{G^2(s')\rho(s')}{s' - s}\right]^{-1}. \tag{B2}$$

Here $\rho(s)$ is the invariant $\pi\pi$ phase space. In the physical region, at $s > 4m_\pi^2$ and s on the upper edge of the threshold cut, we have:

$$\Pi(s) = \int_{4m_\pi^2}^{\infty}\frac{ds'}{\pi}\frac{G^2(s')\rho(s')}{s' - s - i0} = P\int_{4m_\pi^2}^{\infty}\frac{ds'}{\pi}\frac{G^2(s')\rho(s')}{s' - s} + iG^2(s)\rho(s), \tag{B3}$$

with the following relation to the $IJ^{PC} = 00^{++}$ phase shift: $\rho(s)A(s) = \exp(i\delta_0^0(s))\sin\delta_0^0(s)$. The product of the vertices $G^2(s)$ is actually an N function, and we rewrite $G^2(s) \to N(s)$; this allows to present the amplitude (B2) as

$$A(s) = \frac{N(s)}{D(s)}, \quad D(s) = s^2 - \int_{4m_\pi^2}^{\infty}\frac{ds'}{\pi}\frac{\rho(s')N(s')}{s' - s - i0}. \tag{B4}$$

The N function, being determined by the left-hand singularities caused by forces due to t-channel and u-channel meson exchanges, is written as an integral along the left cut as follows:

$$N(s) = \int_{-\infty}^{s_L}\frac{ds'}{\pi}\frac{L(s')}{s' - s}, \tag{B5}$$

where the value s_L marks the beginning of the left-hand cut. For example, for the one-meson exchange diagram $g^2/(m^2 - t)$ the left-hand cut starts at $s_L = 4m_\pi^2 - m^2$, and the N function in this point has a logarithmic singularity; for the two-pion exchange, $s_L = 0$.

We replace the left-hand integral for $N(s)$, Eq. (B5), by the following sum:

$$N(s) = \int_{-\infty}^{s_L}\frac{ds'}{\pi}\frac{L(s')}{s' - s} \to 16\pi\sqrt{s}\sum_n\frac{L_n}{s_n - s}, \tag{B6}$$

where L_n and s_n are "force parameters," $-\infty < s_n < s_L$.

The pole approximation *ansatz* (B6) allows us calculate the scattering amplitude in the physical region:

$$\exp(i\delta_0^0(s))\sin\delta_0^0(s) = \frac{\sqrt{s - 4m_\pi^2}\sum_n L_n(s - s_n)^{-1}}{s^2 - \sum_n(\sqrt{4m_\pi^2 - s_n} + i\sqrt{s - 4m_\pi^2})L_n(s - s_n)^{-1}}. \tag{B7}$$

Such amplitude has only first order poles in the complex plane.

APPENDIX C: THE $\pi\pi$ SCATTERING AMPLITUDE NEAR TWO-PION THRESHOLDS

Here we consider the $\pi\pi$ scattering amplitude near two-pion thresholds taking into account the mass difference of charged and neutral pion systems, $\pi^+\pi^-$ and $\pi^0\pi^0$.

The following $\pi\pi$ amplitudes describe scattering reactions near the thresholds:

$$\pi^+\pi^- \to \pi^+\pi^-\colon A_{--}^{++} = \frac{a_{--}^{++} + ik_0^0[(a_{-0}^{+0})^2 - a_{--}^{++}a_{00}^{00}]}{1 - ik_-^+a_{--}^{++} - ik_0^0a_{00}^{00} + k_0^0k_-^+[-a_{00}^{00}a_{--}^{++} + (a_{-0}^{0+})^2]},$$

$$\pi^0\pi^0 \to \pi^+\pi^-\colon A_{0-}^{0+} = \frac{a_{0-}^{0+}}{1 - ik_-^+a_{--}^{++} - ik_0^0a_{00}^{00} + k_0^0k_-^+[-a_{00}^{00}a_{--}^{++} + (a_{0-}^{0+})^2]},$$

$$\pi^0\pi^0 \to \pi^0\pi^0\colon A_{00}^{00} = \frac{a_{00}^{00} + ik_-^+[(a_{-0}^{+0})^2 - a_{--}^{++}a_{00}^{00}]}{1 - ik_-^+a_{--}^{++} - ik_0^0a_{00}^{00} + k_0^0k_-^+[-a_{00}^{00}a_{--}^{++} + (a_{-0}^{0+})^2]},$$

$$\text{with} \quad k_-^+ = \sqrt{\frac{s}{4} - m_\pi^2} \equiv k, \qquad k_0^0 = \frac{1}{2}\sqrt{\frac{s}{4} - m_{\pi^0}^2} = \frac{1}{2}\sqrt{k^2 + \Delta^2}. \tag{C1}$$

Here $\Delta^2 = m_\pi^2 - m_{\pi^0}^2 \simeq 0.07 m_{\pi^+}^2$. The factor $1/2$ in k_0^0 arises due to the identity of pions in the $\pi^0\pi^0$ state.

We impose on the scattering length values the standard isotopic relations:

$$a_{--}^{++} = \tfrac{2}{3}a_0(s) + \tfrac{1}{3}a_2(s), \qquad a_{-0}^{+0} = -\tfrac{2}{3}a_0(s) + \tfrac{2}{3}a_2(s), \qquad a_{00}^{00} = 2a_{--}^{++} + a_{-0}^{+0} = \tfrac{2}{3}a_0(s) + \tfrac{4}{3}a_2(s). \tag{C2}$$

Then at large k^2, when $k^2 \gg \Delta^2$, the unitary amplitudes of Eq. (C1) obey the isotopic relations:

$$\begin{aligned} A_{--}^{++} &= \frac{\frac{2}{3}a_0(s)}{1 - ika_0(s)} + \frac{\frac{1}{3}a_2(s)}{1 - ika_2(s)}, \\ A_{-0}^{+0} &= \frac{-\frac{2}{3}a_0(s)}{1 - ika_0(s)} + \frac{\frac{2}{3}a_2(s)}{1 - ika_2(s)}, \\ A_{00}^{00} &= \frac{\frac{2}{3}a_0(s)}{1 - ika_0(s)} + \frac{\frac{4}{3}a_2(s)}{1 - ika_2(s)}. \end{aligned} \tag{C3}$$

The $(I = 0)$ amplitude and the corresponding S-matrix read:

$$\begin{aligned} \frac{a_0(s)}{1 - ika_0(s)} &= 2A_{--}^{++} - \frac{1}{2}A_{00}^{00} = A_{--}^{++} - \frac{1}{2}A_{-0}^{+0}, \\ \exp[2i\delta_0^0(s)] &= \frac{A_{--}^{++} - \frac{1}{2}A_{-0}^{+0}}{(A_{--}^{++} - \frac{1}{2}A_{-0}^{+0})^*} = \frac{A_{--}^{++} - \frac{1}{2}A_{-0}^{+0}}{(2A_{--}^{++} - \frac{1}{2}A_{00}^{00})^*} \\ &= \frac{2A_{--}^{++} - \frac{1}{2}A_{00}^{00}}{(2A_{--}^{++} - \frac{1}{2}A_{00}^{00})^*}. \end{aligned} \tag{C4}$$

In the $K^+ \to e^+\nu(\pi^+\pi^-)$ decay the S-wave pions are $I = 0$ states, and the amplitude can be written as follows:

$$\begin{aligned} &A(K^+ \to e^+\nu(\pi^+\pi^-)_{I=0,S\text{-wave}}) \\ &\quad = \lambda[1 - ik_0^0 A_{0-}^{0+} + ik_-^+ A_{--}^{++}] \\ &\quad = \lambda\frac{1 - ik_0^0 a_{00}^{00} - ik_0^0 a_{0-}^{0+}}{1 - ik_-^+ a_{--}^{++} - ik_0^0 a_{00}^{00} + k_0^0 k_-^+[-a_{00}^{00} a_{--}^{++} + (a_{0-}^{0+})^2]}. \end{aligned} \tag{C5}$$

Here the first term, λ, is a direct production amplitude while the second and third terms take into account pion rescatterings.

At large pion relative momentum, when $k^2 \gg \Delta^2$, we have:

$$A(K^+ \to e^+\nu(\pi^+\pi^-)_{I=0,S\text{-wave}})_{k^2 \gg \Delta^2} = \lambda\frac{1}{1 - ika_0(s)}. \tag{C6}$$

Recall that the factor $(1 - ika_0(s))^{-1}$ is due to rescatterings of pions in the $I = 0$ state.

A very similar investigation with taken into account of the isospin violation in a more sophisticated way can be found in [38].

[1] K. Nakamura *et al.* (Particle Data Group), J. Phys. G **37**, 075021 (2010).
[2] M. Ablikim *et al.* (BES Collab.) Phys. Lett. B **645**, 19 (2007).
[3] R. Garcia-Martin, J. R. Pelaez, and F. J. Yndurain, Phys. Rev. D **76**, 074034 (2007).
[4] D. V. Bugg, J. Phys. G **34**, 151 (2007).
[5] I. Caprini, G. Colangelo, and H. Leutwyler, Phys. Rev. Lett. **96**, 132001 (2006).
[6] I. Caprini, Phys. Rev. D **77**, 114019 (2008).
[7] V. V. Anisovich *et al.* (Crystal Ball Collaboration.), Phys. Lett. B **323**, 233 (1994).
[8] B. Hyams *et al.*, Nucl. Phys. **B64**, 134 (1973).
[9] D. V. Bugg, B. S. Zou, and A. V. Sarantsev, Nucl. Phys. **B471**, 59 (1996).
[10] W. Ochs, AIP Conf. Proc. **1257**, 252 (2010).
[11] M. Albaladejo, J. A. Oller, and C. Piqueras, in *Proceedings of 11th International Conference on Meson-Nucleon Physics and the Structure of the Nucleon (MENU 2007), Julich, Germany, 2007*, p. 203 (unpublished).
[12] V. V. Anisovich and A. V. Sarantsev, Eur. Phys. J. A **16**, 229 (2003); V. V. Anisovich, A. A. Kondashov, Yu. D. Prokoshkin, S. A. Sadovsky, and A. V. Sarantsev, Yad. Fiz. **63**, 1410 (2000) [Phys. At. Nucl. **63**, 1410 (2000)]; V. V. Anisovich and A. V. Sarantsev, Phys. Lett. B **382**, 429 (1996).
[13] V. V. Anisovich and A. V. Sarantsev, Int. J. Mod. Phys. A **24**, 2481, (2009); V. V. Anisovich and A. V. Sarantsev, Yad. Fiz. **72**, 1950 (2009) [Phys. At. Nucl. **72**, 1889 (2009)]; V. V. Anisovich and A. V. Sarantsev, Yad. Fiz. **72**, 1981 (2009) [Phys. At. Nucl. **72**, 1920 (2009)].
[14] V. V. Anisovich, Yu. D. Prokoshkin, and A. V. Sarantsev, Phys. Lett. B **389**, 388 (1996).
[15] A. V. Anisovich, V. V. Anisovich, M. A. Matveev, V. A. Nikonov, J. Nyiri, and A. V. Sarantsev, *Mesons and Baryons* (World Scientific, Singapore, 2008).
[16] V. V. Anisovich and V. A. Nikonov, Eur. Phys. J. A **8**, 401 (2000).
[17] R. Garcia-Martin, R. Kaminski, J. R. Pelaez, J. Ruiz de Elvira, and F. J. Yndurain, Phys. Rev. D **83**, 074004 (2011).
[18] A. V. Anisovich, V. V. Anisovich, Yu. D. Prokoshkin, and A. V. Sarantsev, Z. Phys. A **357**, 123 (1997).
[19] A. V. Anisovich, V. V. Anisovich, and A. V. Sarantsev, Phys. Lett. B **395**, 123 (1997); Z. Phys. A **359**, 173 (1997).
[20] I. S. Shapiro, Nucl. Phys. **A122**, 645 (1968).

[21] I. Yu. Kobzarev, N. N. Nikolaev, and L. B. Okun, Yad. Fiz. **10**, 864 (1969).
[22] L. Stodolsky, Phys. Rev. D **1**, 2683 (1970).
[23] V. V. Anisovich, D. V. Bugg, and A. V. Sarantsev, Phys. Rev. D **58**, 111503 (1998).
[24] V. V. Anisovich, L. G. Dakhno, M. A. Matveev, V. A. Nikonov, and A. V. Sarantsev, Yad. Fiz. **70**, 480 (2007) [Phys. At. Nucl. **70**, 450 (2007)]; arXiv:hep-ph/0511109.
[25] V. V. Anisovich, L. G. Dakhno, M. A. Matveev, V. A. Nikonov, and A. V. Sarantsev, Yad. Fiz. **70**, 68 (2007) [Phys. At. Nucl. **70**, 63 (2007)]; arXiv:hep-ph/0510410.
[26] V. V. Anisovich, L. G. Dakhno, M. A. Matveev, V. A. Nikonov, and A. V. Sarantsev, Yad. Fiz. **70**, 392 (2007) [Phys. At. Nucl. **70**, 364 (2007)]; arXiv:hep-ph/0511105.
[27] A. V. Anisovich, V. V. Anisovich, L. G. Dakhno, M. A. Matveev, V. A. Nikonov, and A. V. Sarantsev, J. Phys. G **37**, 025004 (2010); V. V. Anisovich, L. G. Dakhno, M. A. Matveev, V. A. Nikonov, and A. V. Sarantsev, Yad. Fiz. **73**, 488 (2010) [Phys. At. Nucl. **73**, 462 (2010)]; arXiv:hep-ph/0901.4854.
[28] E. Salpeter and H. A. Bethe, Phys. Rev. **84**, 1232 (1951).
[29] A. V. Anisovich, V. V. Anisovich, and A. V. Sarantsev, Phys. Rev. D **62**, 051502(R) (2000).
[30] J. Nyiri, *The Gribov Theory of Quark Confinement* (World Scientific, Singapore, 2001).
[31] F. Q. Wu, B. S. Zou, L. Li, and D. V. Bugg, Nucl. Phys. **A735**, 111 (2004).
[32] A. Aloisio *et al.*, Phys. Lett. B **537**, 21 (2002).
[33] V. Cirigliano, G. Ecker, and A. Pich, Phys. Lett. B **679**, 445 (2009).
[34] G. Colangelo, J. Gasser, and H. Leutwyler, Nucl. Phys. **B603**, 125 (2001).
[35] V. V. Anisovich, V. A. Nikonov, and A. V. Sarantsev, Yad. Fiz. **66**, 772 (2003) [Phys. At. Nucl. **66**, 741 (2003)].
[36] G. F. Chew and S. Mandelstam, Phys. Rev. **119**, 467 (1960).
[37] G. F. Chew, *The Analytic S-Matrix* (W. A. Benjamin, New York, 1966).
[38] G. Colangelo, J. Gasser, and A. Rusetsky, Eur. Phys. J. C **59**, 777 (2008).
[39] V. V. Anisovich, Usp. Fiz. Nauk **168**, 481 (1998); [Phys. Usp. **41**, 419 (1998)].